Supplementary Information

Metastable States in the Hinge-Bending Landscape of an Enzyme in an Atomistic Cytoplasm Simulation

Premila P. Samuel Russell[†], Andrew K. Maytin[‡], Meredith M. Rickard[†], Matthew C. Russell[%], Taras V. Pogorelov[†,§,#,&,^,*], and Martin Gruebele[†,§,&,‡,*]

[†]Department of Chemistry, [‡]Department of Physics, [%]Department of Mathematics, [§]Center for Biophysics and Computational Biology, [#]School of Chemical Sciences, [&]Beckman Institute for Advanced Science and Technology, [‡]Carle-Illinois College of Medicine, and [^]National Center for Supercomputing Applications, University of Illinois Urbana-Champaign, Urbana, Illinois 61801, USA

[*]Corresponding author emails: pogorelo@illinois.edu, mgruebel@illinois.edu

SI Methods. The human cell cytoplasm models were constructed and equilibrated for simulations as described in our previous works[1,2]. The specific solute content for each cytoplasm model used in present work is are listed in Tables S3-S6. The yPGK variant used in our simulations had R65Q/W333F mutations. For the simulations in dilute water boxes, the initial structure was generated using AlphaFold2 (with Colab notebook)[3], with the initial hinge-bending angles of hPGK being 109°. The simulations in the dilute water boxes contained 0.15 M NaCl. The cytoplasm models and models of dilute water boxes were parameterized using CHARMM TIP3P[4] water for solvent, Beglov and Roux's parameters[5] for inorganic ions, and CHARMM36m[6] for proteins. The cytoplasm models were additionally parameterized using CHARMM36 additive for lipids, CHARMM36 additive for nucleic acids, and CGENFF[7] for metabolites. All simulations were conducted as isothermal-isobaric ensembles, at 318 K, 1 atm pressure, 2 femto-seconds time-steps, and under periodic boundary conditions. Productions runs of cytoplasm models were conducted on the Anton 2 supercomputer (Pittsburgh Supercomputer Center) with a multigrator[8] scheme while the dilute water box simulations were conducted using NAMD3 software[9]. CPPTRAJ[10] software was used to measure hinge-bending angles. Hinge-bending angle trajectories analyzed had intervals of 2.4 ns between sequential data points.

Transitions at time t_m between two STaSI states were characterized using piecewise logistic functions (Eq. 1):

$$\theta(t) = \theta_i + \frac{\theta_j - \theta_i}{1+\exp\left(-k^{\dagger}(t-t_m)\right)}, \quad [1]$$

where $\theta_i$and θ_j are the start and endpoints of a state and $k^{\dagger}$ is the passage rate. The logistic function fits to the STaSI transitions between states were used to derive the transition midpoints t_{m1}-t_{m7} in Fig. 1B,C. For the transition around midpoint t_{m8}, the logistic function could not be applied due to rapid fluctuations on the angle centroids. Here t_{m8} was taken as the midpoint between ending and beginning of two sequential longest time periods of the clustered Open state ensembles, with the break in the ensemble continuity was only taken account for time lengths larger than 120 ns.

VMD[11] scripts were used to calculate ligand binding to active site residues of hPGK and yPGK. Binding calculations were done following wrapping of the simulation trajectories of PGK and the substrate ligands, centered around the center of mass of PGK, using the PBCtools plugin for VMD v3.1[12]. We counted binding to occur when substrates are within 0.45 nm of their respective active site residues on hPGK. ADP/ATP active site on hPGK was defined as residues: 212-215, 219, 237, 238, 241, 256, 291, 312, 313, 336-343, 371-375, 395, and 396; and on yPGK was defined as residues: 210-213, 217, 235, 236, 239, 254, 289, 310-312, 334-341, and 370-373. 1,3-BPG/3PG active site on hPGK was defined as residues 23, 25, 38, 62, 64, 65, 122, 166, 167, 169, 170, and 172. AutoDock Vina software[13] was used to dock 1,3-BPG and ADP onto their respective active sites in hPGK.

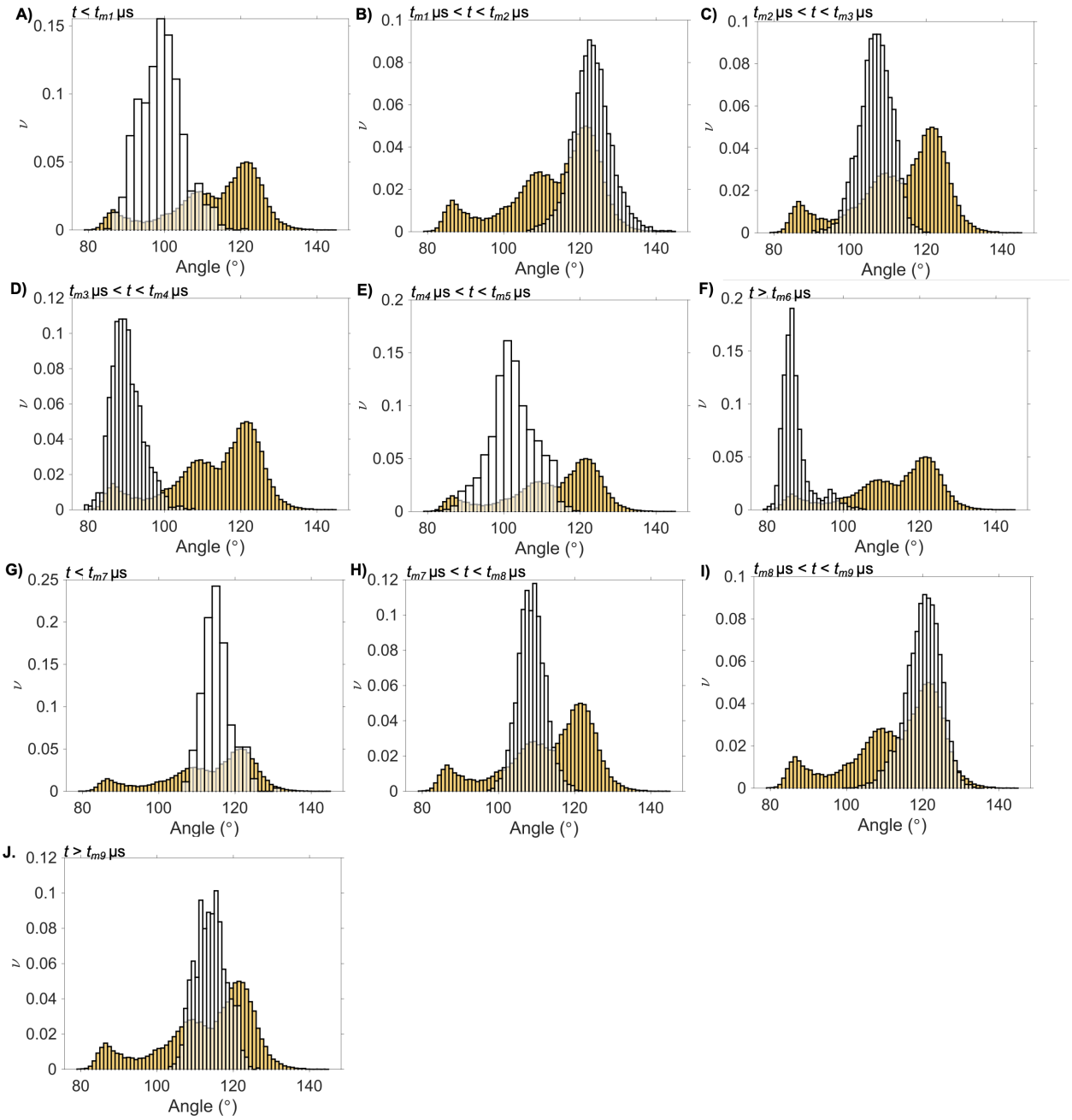

Figure S1. Hinge-bending angle distribution and frequency (ν) for hPGK in the cell cytoplasm model. The yellow rectangles represent overall angle distribution across the hinge-bending angle trajectories (Fig. 1BC) for both CellA and CellB (for initial placement of hPGK in the apo state). The white rectangles represent the angle distribution for segments of *t* time ranges of CellA or CellB simulation trajectories as described above each specific plot. For calculations of both ensemble dwell times and plotting of hinge bending angle energy plot, we defined angles distributions of (B),(I) as Open state ensembles; (C),(E),(H) as Semi-Open state ensembles; and (D) as Closed ensembles.

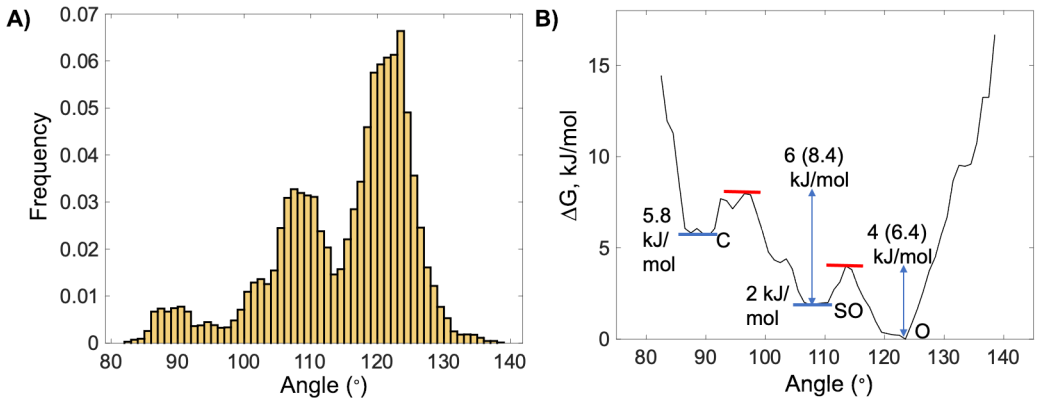

Figure S2. Energy landscape exploration for hPGK hinge-bending dynamics within the human cell using frequency distribution. (A) Histogram $P(\theta)$ of the hinge-bending angles, and (B) free energy diagram - $RT\ln(P)$ for hinge-bending ensemble states in hPGK simulated within human cytoplasm models. The hinge-bending angles evaluated here are those occurring in Fig. 2B within t_{m1} to t_{m5} time-points during CellA trajectory, and in Fig. 2B within t_{m6} to t_{m8} time-points during CellB trajectory in order to be consistent with the Energy plot in Fig. 2A. A Gaussian smoothing filter with 24 ns window was applied to the frequency distribution in A, and the energy plot in B was then evaluated for the smoothed data. Energy barriers in bracket represent barrier values corrected for the underestimated water model viscosity. Note that the barriers here are likely too low due to θ not being an accurate reaction coordinate near the saddle points for the transitions, thus overestimating the flux between states. We recommend the higher values based on STaSI analysis in Fig. 2 of the main text as our best estimates of free energy barriers.

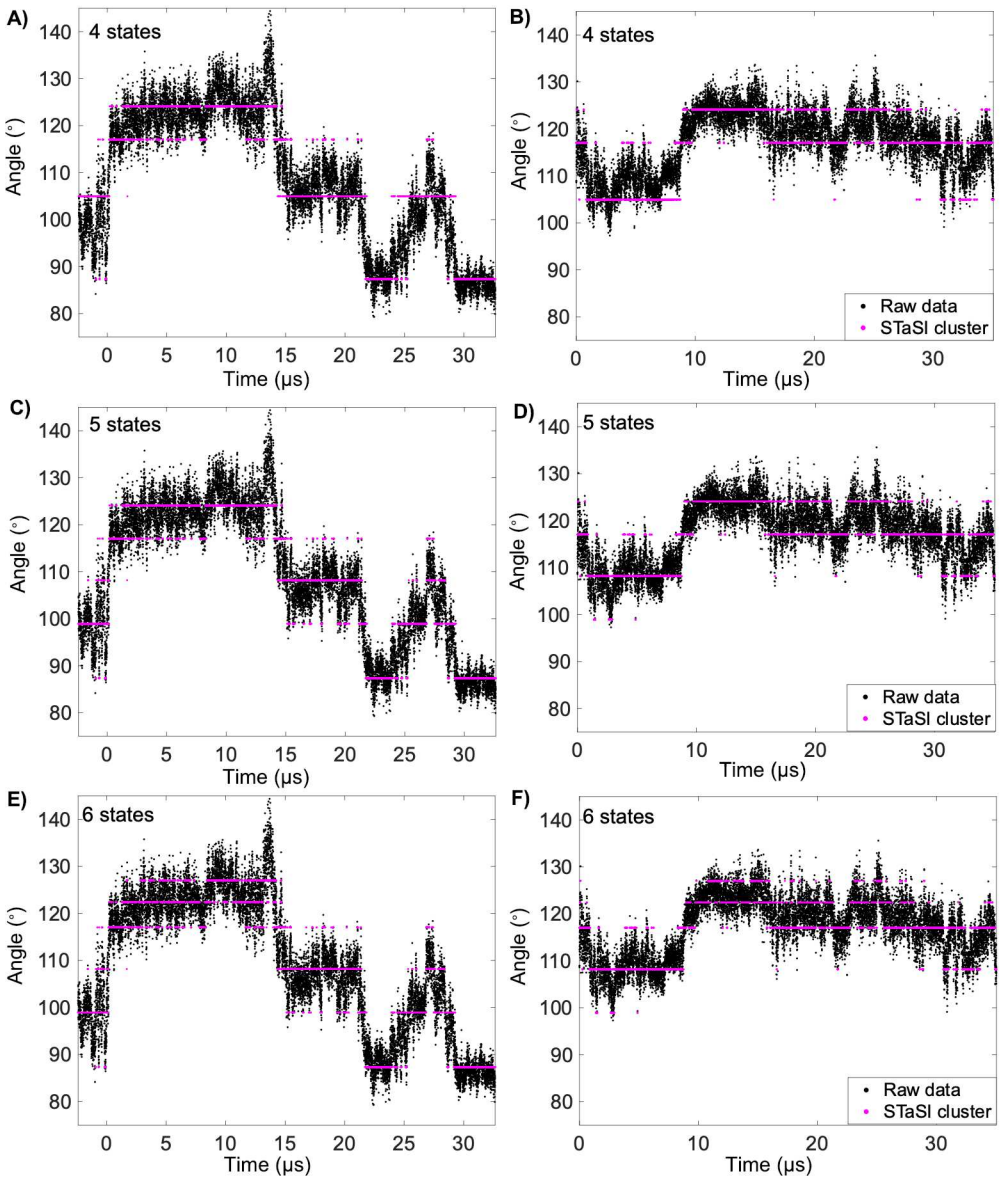

Figure S3. Clustering of hinge-bending angle trajectories of hPGK, simulated with the cell cytoplasm models, into 4-state, 5-state, and 6-state ensembles.

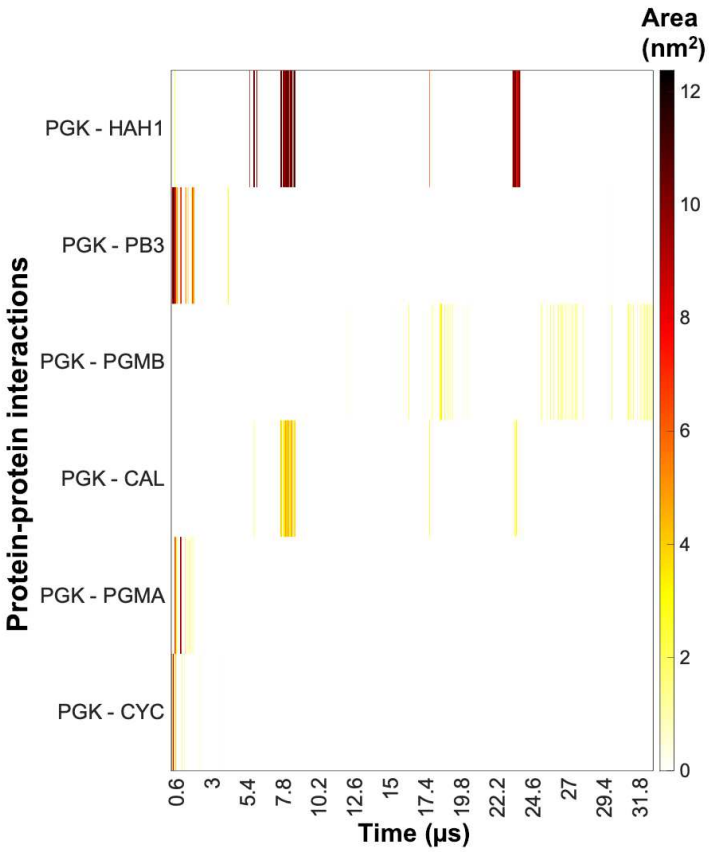

Figure S4. The six overall largest protein-protein interactions in terms contact area involving hPGK in CellA shown for simulation times between 0.24 μs and 32.6 μs. Protein abbreviations are as following: PB3 – Protein B (copy 3); PGMA/B – phosphoglycerate mutase subunit A/B; and CYC – cyclophilin G.

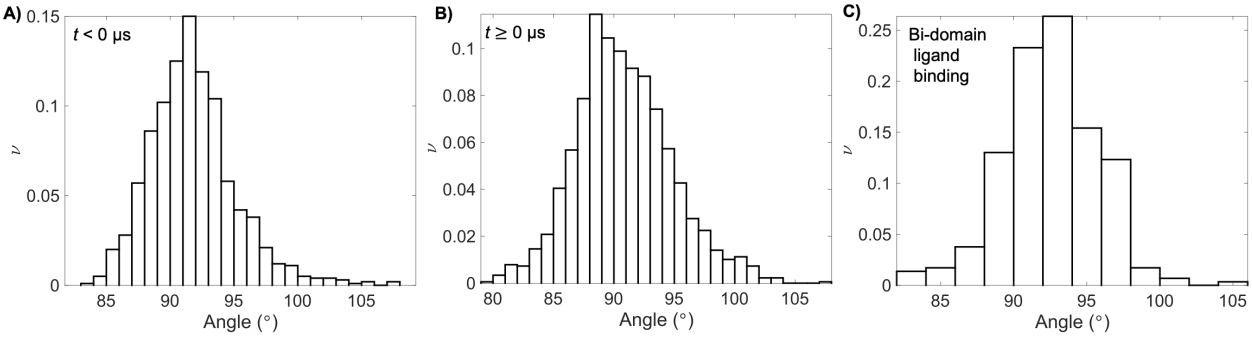

Figure S5. Hinge-bending angle distribution and frequency (ν) for hPGK in the cell cytoplasm model following bi-domain ligand docking. (A) and (B) represent the distributions during time t for $t < 0$ μs and ≥ 0 μs respectively along the trajectory in Fig. 3A. Frequent ligand binding and disassociation was seen occurring more during $t < 0$ μs, and consequently there are variability in the angle distribution between histograms in (A) and (B). (C) Histogram of angle distribution during bi-domain ligand binding in hPGK.

Table S1. Parameters for hPGK hinge-bending landscape in Fig. 1 as determined using logistic function.

Parameter	Time point	Value
$k^{\dagger}_{SO\_O}$	centered at t_{m1}	-*
$k^{\dagger}_{O\_SO}$	centered at t_{m2}	4.8 μs^{-1}
$k^{\dagger}_{SO\_C}$	centered at t_{m3}	6.9 μs^{-1}
$k^{\dagger}_{C\_SO}$	centered at t_{m4}	1.7 μs^{-1}
$k^{\dagger}_{SO\_C}$	centered at t_{m5}	3.4 μs^{-1}
$k^{\dagger}_{O\_SO}$	centered at t_{m6}	1.4 μs^{-1}
$k^{\dagger}_{SO\_O}$	centered at t_{m7}	1.3 μs^{-1}
Average $k^{\dagger}$ ± normal error		3.3±0.9 μs^{-1}
O dwell rate	between t_{m1} and t_{m2}	0.0685 μs^{-1}
O dwell rate	between t_{m7} and t_{m8}	0.0418 μs^{-1}
Average O dwell rate ± normal error		0.0552±0.0134 μs^{-1}
SO dwell rate	between t_{m2} and t_{m3}	0.147 μs^{-1}
SO dwell rate	between t_{m4} and t_{m5}	0.278 μs^{-1}
SO dwell rate	between t_{m6} and t_{m7}	0.137 μs^{-1}
Average SO dwell rate ± normal error		0.187±0.045 μs^{-1}
C dwell rate	between t_{m3} and t_{m4}	0.286 μs^{-1}

*This value could not be determined accurately due to a rapid transition to a substate with smaller angle than the SO state.

Summary of error propagation using Table S1:
$k = k^{\dagger} * \exp(-\Delta G^{\dagger}/RT)$
$\Delta G^{\dagger} = -RT\ln(k/k^{\dagger})$
$\Delta G = -RT\ln(K_{eq}) = -RT\ln(k_f/k_b)$

For $\ln(a/b)$, the error range assuming no parameter correlation, and analogous derivative propagation are
$\{\ln((a+da)/(b-db)) - \ln((a-da)/(b+db))\}$ (full range) → $\pm (adb + bda)/ab$ (derivative)
$\Delta G^{\dagger}$, O to SO:
-0.00831*318*ln((0.0552±0.0134) / (3.3∓0.9)) =10.8±1.4 kJ/mol
where 0.00831*318*(0.0552*0.9 + 3.3*0.0134)/(0.0552*3.3) ≈ 1.4
$\Delta G^{\dagger}$, SO to C:
-0.00831*318*ln((0.187±0.045) / (3.3∓0.9)) =7.6±1.4 kJ/mol
where 0.00831*318*(0.187*0.9 + 3.3*0.045)/(0.187*3.3) ≈ 1.4
ΔG, O to SO:
-0.00831*318*ln((0.0552±0.0134) / (0.187∓0.045)) = 3.2±1.3 kJ/mol
where 0.00831*318*(0.0552*0.045 + 0.187*0.0134)/(0.187*0.0552) ≈ 1.3

$\tau^{\dagger} = 1/k^{\dagger} = 1/(3.3\pm0.9) \approx 0.3\pm0.1$ μs; viscosity corrected by 2.5 gives 0.8±0.3 μs.

Table S2. Parameters for yPGK hinge-bending landscape in Fig. 5 as determined using logistic function.

Parameter	Time point	Value
$k^{\dagger}_{O\_SO}$	centered at t_{mi}	11.6 μs^{-1}
$k^{\dagger}_{SO\_C}$	centered at t_{mii}	14.9 μs^{-1}
$k^{\dagger}_{C\_SO}$	centered at t_{miii}	2.6 μs^{-1}
Average $k^{\dagger} \pm$ normal error		9.7 $\pm$ 3.7 μs^{-1}

Normal errors were evaluated as $NE = [s^2/N]^{1/2}$, $s^2 = \Sigma (x_i - \langle x_i \rangle)^2/(N-1)$

Table S3. Metabolites present in CellA cytoplasm model

Metabolite	**Concentration in Model (mM)**
Glutamate	34.87
Taurine	21.26
Aspartate	17.86
Glutamine	11.06
Glycine	11.06
Glutathione (GSH)	5.10
Spermine	4.25
Lactate	4.25
Asparagine	1.70
Malate	8.50
Alanine	5.10
Spermidine	1.70
Beta-Alanine	3.40
Citrate/Isocitrate	5.95
Hydroxyproline	3.40
ATP	1.70
Putrescine	0.85
Phosphocholine	2.55
UTP	3.40
Isoleucine	0.85
NAD	1.70
Serine	1.70
Leucine	0.85
Threonine	1.70

Arginine	3.40
Histidine	0.85
Valine	0.85
Glutathione disulfide (GSSG)	0.85
UDP	0.85
Tyrosine	0.85
3-Hydroxybutyric acid	1.70
Glycerol-3-phosphate (G3P)	0.85
Fumarate	0.85
GTP	0.85
ADP	1.70
AMP	0.85
Fructose-1,6-bisphosphate	0.85
Succinate	0.85
Pyruvate	0.85
Ribose-5-phosphate/ ribulose-5-phosphate	0.85
Pantothenic Acid	0.85
Glucose-6-phosphate (G6P)	0.85
Citrulline	0.85
GMP	0.85

Table S4. Metabolites present in CellB cytoplasm model

Metabolite	**Concentration in Model (mM)**
Glutamate	27.13
Taurine	12.27
Aspartate	11.63
Glutamine	9.69
Glycine	14.21
GSH	3.88
Spermine	5.81
Lactate	2.58
Asparagine	1.29
Malate	1.94
Alanine	1.29

Spermidine	1.29
Beta-alanine	3.23
Citrate/Isocitrate	1.94
Proline	1.29
Hydroxyproline	1.94
ATP	1.94
Putrescine	2.58
Phosphocreatine	1.29
Phosphocholine	2.58
UTP	0.65
Isoleucine	2.58
NAD	1.29
Leucine	0.65
Threonine	2.58
Creatine	0.65
Arginine	1.29
Histidine	1.29
Valine	0.65
Alpha-ketoglutarate	1.29
UDP-hexose	1.94
Tyrosine	1.29
Lysine	0.65
3-Hydroxybutyric acid	1.29
G3P	0.65
UMP	1.29
ADP	0.65
Choline	0.65
FBP	1.94
CTP	1.94
CMP	1.29
Adenine	0.65
3PG	1.29
dTTP	1.29
Carnitine	0.65
Acetylserine	0.65
Glycerophosphocholine	1.29

GABA	0.65
GDP	0.65

Table S5. Inorganic ions present in the cytoplasm models

Ion	Concentration in CellA (mM)	Concentration in CellB (mM)
K^+	157.3	155.6
Na^+	4.25	3.87
Mg^{2+}	8.50	8.39
Cl^-	11.0	5.16

Table S6. Macromolecules present in the cytoplasm models

Molecule |Cytoplasm model(s)| | Copies in each model | Protein quaternary state	Protein /nucleotide sequence per subunit
Cyclophilin G | CellA | 1 | Monomer	RPRCFFDIAINNQPAGRVVFELFSDVCPKTCENFRCLCTGEKGTGKSTQKPLHYKSCLFH RVVKDFMVQGGDFSEGNGRGGESIYGGFFEDESFAVKHNAAFLLSMANRGKDTNGSQFFI TTKPTPHLDGHHVVFGQVISGQEVVREIENQKTDAASKPFAEVRILSCGELIP
Calmodulin | CellA and CellB | 1(CellA) and 1(CellB) | Monomer	MADQTEEQIAEFKEAFSLFDKDGDGTITTKELGTVMRSLGQNPTEAELQDMINEVDADGN GTIDFPEFLTMMARKMKDTDSEEEIREAFRVFDKDGNGYISAAELRHVMTNLGEKLTDEE VDEMIREADIDGDGQVNYEEFVQMMTAK
tRNA | CellA and CellB | 1(CellA) and 1(CellB)	GACCUCGUGGCGCAAUGGUAGCGCGUCUGACUCCAGAUCAGAAGGUUGCGUGUUCGAAUCA CGUCGGGGUCA
GAPDH| CellA | 1 | Tetramer	MGKVKVGVNGFGRIGRLVTRAAFNSGKVDIVAINDPFIDLNYMVYMFQYDSTHGKFHGTV KAENGKLVINGNPITIFQERDPSKIKWGDAGAEYVVESTGVFTTMEKAGAHLQGGAKRVI ISAPSADAPMFVMGVNHEKYDNSLKIISNASCTTNCLAPLAKVIHDNFGIVEGLMTTVHA ITATQKTVDGPSGKLWRDGRGALQNIIPASTGAAKAVGKVIPELNGKLTGMAFRVPTANV SVVDLTCRLEKPAKYDDIKKVVKQASEGPLKGILGYTEHQVVSSDFNSDTHSSTFDAGAG IALNDHFVKLISWYDNEFGYSNRVVDLMAHMASKE
HAH1 | CellA and CellB | 1(CellA) and 1(CellB) | Monomer	MPKHEFSVDMTCGGCAEAVSRVLNKLGGVKYDIDLPNKKVCIESEHSMDTLLATLKKTGK TVSYLGLE
PGM | CellA and CellB | 1(CellA) and	MAAYKLVLIRHGESAWNLENRFSGWYDADLSPAGHEEAKRGGQALRDAGYEFDICFTSVQ KRAIRTLWTVLDAIDQMWLPVVRTWRLNERHYGGLTGLNKAETAAKHGEAQVKIWRRSYD VPPPPMEPDHPFYSNISKDRRYADLTEDQLPSCESLKDTIARALPFWNEEIVPQIKEGKR VLIAAHGNSLRGIVKHLEGLSEEAIMELNLPTGIPIVYELDKNLKPIKPMQFLGDEETVR KAMEAVAAQGKAKK

1(CellB) | Dimer	
Protein B | CellA | 3(CellA) | Monomer	LKNAIEDAIAEWKKAGITSDFYFNAINKAKTVEEVNALVNEILKAHA
hPGK | CellA and CellB | 1(CellA) and 1(CellB) | Monomer	MSLSNKLTLDKLDVKGKRVVMRVDFNVPMKNNQITNNQRIKAAVPSIKFCLDNGAKSVVL MSHLGRPDGVPMPDKYSLEPVAVELKSLLGKDVLFLKDCVGPEVEKACANPAAGSVILLE NLRFHVEEEGKGKDASGNKVKAEPAKIEAFRASLSKLGDVYVNDAFGTAHRAHSSMVGVN LPQKAGGFLMKKELNYFAKALESPERPFLAILGGAKVADKIQLINNMLDKVNEMIIGGGM AFTFLKVLNNMEIGTSLFDEEGAKIVKDLMSKAEKNGVKITLPVDFVTADKFDENAKTGQ ATVASGIPAGWMGLDCGPESSKKYAEAVTRAKQIVWNGPVGVFEWEAFARGTKALMDEVV KATSRGCITIIGGGDTATCCAKWNTEDKVSHVSTGGGASLELLEGKVLPGVDALSNI
Ubiquitin | CellB | 1 | Monomer	MQIFVKTLTGKTITLEVEPSDTIENVKAKIQDKEGIPPDQQRLIFAGKQLEDGRTLSDYNIQKESTLHL VLRLRGG
Cyclophilin A | CellB | 1 | Monomer	VNPTVFFDIAVDGEPLGRVSFELFADKVPKTAENFRALSTGEKGFGYKGSCFHRIIPGFMCQG GDFTRHNGTGGKSIYGEKFEDENFILKHTGPGILSMANAGPNTNGSQFFICTAKTEWLDGKHV VFGKVKEGMNIVEAMERFGSRNGKTSKKITIADCGQLE
GTT WW domain | Cell B | 1 | Monomer	KLPPGWEKRMSRDGRVYYFNHITGTTQFERPSG
HYPK | CellB | 1 | Monomer	MRRRGEIDMATEGDVELELETETSGPERPPEKPRKHDSGAADLERVTDYAEEKEIQSSNL ETAMSVIGDRRSREQKAKQEREKELAKVTIKKEDLELIMTEMEISRAAAERSLREHMGNV VEALIALTN
cAMP dependent protein kinase inhibitor alpha | CellB | 1 | Monomer	MTDVETTYADFIASGRTGRRNAIHDILVSSASGNSNELALKLAGLDINKTEGEEDAQRSS TEQSGEAQGEAAKSES
Thioredoxin | CellB | 1 | Monomer	MVKQIESKTAFQEALDAAGDKLVVVDFSATWCGPCKMIKPFFHSLSEKYSNVIFLEVDVD DCQDVASECEVKCMPTFQFFKKGQKVGEFSGANKEKLEATINELV
Inorganic pyrophosphatase | CellB | 1 | Dimer	MSFSTEERAAPFSLEYRVFLKNEKGQYISPFHDIPIYADKDVFHMVVEVPRWSNAKMEI ATKDPLNPIKQDVKKGKLRYVANLFPYKGYIWNYGAIPQTWEDPGHNDKHTGCCGDNDPI DVCEIGSKVCARGEIIGVKVLGILAMIDEGETDWKVIAINVDDPDAANYNDINDVKRLKP GYLEATVDWFRRYKVPDGKPENEFAFNAEFKDKDFAIDIIKSTHDHWKALVTKKTNGKGI SCMNTTLSESPFKCDPDAARAIVDALPPPCESACTVPTDVDKWFHN
Hsp40 | CellB | 1 | Monomer	MGKDYYQTLGLARGASDEEIKRAYRRQALRYHPDKNKEPGAEEKFKEIAEAYDVLSDPRK REIFDRYGEEGLKGSGPSGGSGGGANGTSFSYTFHGDPHAMFAEFFGGRNPFDTFFGQRN GEEGMDIDDPFSGFPMGMGGFTNVNFGRSRSAQEPARKKQDPPVTHDLRVSLEEIYSGCT KKMKISHKRLNPDGKSIRNEDKILTIEVKKGWKEGTKITFPKEGDQTSNNIPADIVFVLK DKPHNIFKRDGSDVIYPARISLREALCGCTVNVPTLDGRTIPVVFKDVIRPGMRRKVPGE GLPLPKTPEKRGDLIIEFEVIFPERIPQTSRTVLEQVLPI
Hsc70 | CellB | 1 | Monomer	MSKGPAVGIDLGTTYSCVGVFQHGKVEIIANDQGNRTTPSYVAFTDTERLIGDAAKNQVA MNPTNTVFDAKRLIGRRFDDAVVQSDMKHWPFMVVNDAGRPKVQVEYKGETKSFYPEEVS SMVLTKMKEIAEAYLGKTVTNAVVTVPAYFNDSQRQATKDAGTIAGLNVLRIINEPTAAA IAYGLDKKVGAERNVLIFDLGGGTFDVSILTIEDGIFEVKSTAGDTHLGGEDFDNRMVNH

	FIAEFKRKHKKDISENKRAVRRLRTACERAKRTLSSSTQASIEIDSLYEGIDFYTSITRA RFEELNADLFRGTLDPVEKALRDAKLDKSQIHDIVLVGGSTRIPKIQKLLQDFFNGKELN KSINPDEAVAYGAAVQAAILSGDKSENVQDLLLLDVTPLSLGIETAGGVMTVLIKRNTTI PTKQTQTFTTYSDNQPGVLIQVYEGERAMTKDNNLLGKFELTGIPPAPRGVPQIEVTFDI DANGILNVSAVDKSTGKENKITITNDKGRLSKEDIERMVQEAEKYKAEDEKQRDKVSSKN SLESYAFNMKATVEDEKLQGKINDEDKQKILDKCNEIINWLDKNQTAEKEEFEHQQKELE KVCNPIITKLYQSAGGMPGGMPGGFPGGGAPPSGGASSGPTIEEVD

SI References

(1) Samuel Russell, P. P.; Rickard, M. M.; Boob, M.; Gruebele, M.; Pogorelov, T. V. In Silico Protein Dynamics in the Human Cytoplasm: Partial Folding, Misfolding, Fold Switching, and Non-Native Interactions. *Protein Sci.* **2023**, *32*, e4790.

(2) Samuel Russell, P. P.; Rickard, M. M.; Pogorelov, T. V.; Gruebele, M. Metabolons, quinary structure, and domain motion: enzyme choreography in the cytoplasm. https://www.biorxiv.org/content/10.1101/2022.09.13.507800v1 (accessed 2022-09-16).

(3) Jumper, J.; Evans, R.; Pritzel, A.; Green, T.; Figurnov, M.; Ronneberger, O.; Tunyasuvunakool, K.; Bates, R.; Žídek, A.; Potapenko, A.; Bridgland, A.; Meyer, C.; Kohl, S. A. A.; Ballard, A. J.; Cowie, A.; Romera-Paredes, B.; Nikolov, S.; Jain, R.; Adler, J.; Back, T.; Petersen, S.; Reiman, D.; Clancy, E.; Zielinski, M.; Steinegger, M.; Pacholska, M.; Berghammer, T.; Bodenstein, S.; Silver, D.; Vinyals, O.; Senior, A. W.; Kavukcuoglu, K.; Kohli, P.; Hassabis, D. Highly Accurate Protein Structure Prediction with AlphaFold. *Nature* **2021**, *596*, 583–589.

(4) Jorgensen, W. L.; Chandrasekhar, J.; Madura, J. D.; Impey, R. W.; Klein, M. L. Comparison of Simple Potential Functions for Simulating Liquid Water. *J. Chem. Phys.* **1983**, *79*, 926–935.

(5) Beglov, D.; Roux, B. Finite Representation of an Infinite Bulk System: Solvent Boundary Potential for Computer Simulations. *J. Chem. Phys.* **1994**, *100*, 9050–9063.

(6) Huang, J.; Rauscher, S.; Nawrocki, G.; Ran, T.; Feig, M.; de Groot, B. L.; Grubmuller, H.; MacKerell, A. D., Jr. CHARMM36m: An Improved Force Field for Folded and Intrinsically Disordered Proteins. *Nat. Methods* **2017**, *14*, 71–73.

(7) Vanommeslaeghe, K.; Hatcher, E.; Acharya, C.; Kundu, S.; Zhong, S.; Shim, J.; Darian, E.; Guvench, O.; Lopes, P.; Vorobyov, I.; Mackerell, A. D. CHARMM General Force Field: A Force Field for Drug-like Molecules Compatible with the CHARMM All-Atom Additive Biological Force Fields. *J. Comput. Chem.* **2010**, *31*, 671–690.

(8) Lippert, R. A.; Predescu, C.; Ierardi, D. J.; Mackenzie, K. M.; Eastwood, M. P.; Dror, R. O.; Shaw, D. E. Accurate and Efficient Integration for Molecular Dynamics Simulations at Constant Temperature and Pressure. *J. Chem. Phys.* **2013**, *139*, 164106.

(9) Phillips, J. C.; Hardy, D. J.; Maia, J. D. C.; Stone, J. E.; Ribeiro, J. V.; Bernardi, R. C.; Buch, R.; Fiorin, G.; Henin, J.; Jiang, W.; McGreevy, R.; Melo, M. C. R.; Radak, B. K.; Skeel, R. D.; Singharoy, A.; Wang, Y.; Roux, B.; Aksimentiev, A.; Luthey-Schulten, Z.; Kale, L. V.; Schulten, K.; Chipot, C.; Tajkhorshid, E. Scalable Molecular Dynamics on CPU and GPU Architectures with NAMD. *J. Chem. Phys.* **2020**, *153*, 044130.

(10) Roe, D. R.; Cheatham, T. E., 3rd. Parallelization of CPPTRAJ Enables Large Scale Analysis of Molecular Dynamics Trajectory Data. *J. Comput. Chem.* **2018**, *39*, 2110–2117.

(11) Humphrey, W.; Dalke, A.; Schulten, K. VMD: Visual Molecular Dynamics. *J. Mol. Graph* **1996**, *14*, 33–38, 27–28.

(12) Giorgino, T.; Henin, J.; Hoermann, J.; Kulke, M.; Lenz, O.; Mura, C.; Rogers, D. M.; Saam, J. PBCTools v3.0, 2023. https://github.com/frobnitzem/pbctools (accessed 2023-11-01).

(13) Trott, O.; Olson, A. J. AutoDock Vina: Improving the Speed and Accuracy of Docking with a New Scoring Function, Efficient Optimization and Multithreading. *J. Comput. Chem.* **2010**, *31*, 455–461.